TECHNISCHE
UNIVERSITÄT
WIEN
Vienna University of Technology

Projektarbeit

Electrochemical Cell For Single Crystal Samples

Ausgeführt am Institut für Angewandte Physik
der Technischen Universität Wien

unter der Anleitung von
ASSOZ.Prof. Gareth S. Parkinson, PhD
und
Dr.techn. Jiří Pavelec

durch
Claus Kovacs

Abstract

Understanding the flow properties and mass transport through an electrochenical flow cell is crucial for optimizing its design. In the scope of this project work, simulations with the program Comsol were performed to investigate these phenomena. Stationary and time-dependent studies were performed utilizing the Comsol modules laminar flow and transport of diluted species. The results of this project work can be used to optimize an electrochemical flow cell regarding flow and mass transport.

Zusammenfassung

-

Contents

1 Introduction **1**
1.1 Flow . . . 3
1.1.1 Reynolds Number . . . 3
1.1.2 Boundary Layers . . . 4
1.1.3 Darcy–Weisbach Equation . . . 5
1.1.4 Residence Time Distributions . . . 5
1.2 Comsol . . . 6
1.2.1 Convergence . . . 7

2 Simulations / Results **9**
2.1 Cell Design . . . 9
2.2 Pressure / Velocity Study . . . 10
2.3 Mass Transport Study . . . 16

3 Conclusions **23**

List of Figures

1 Schematic of the electrochemical flow cell 1
2 Schematic of the vapor pressure pumping system 2
3 Vapor pressure of water according to the Antoine equation. 3
4 Boundary layer development over a flat plane 4
5 Schematic of the flow cell 9
6 Mesh convergence for stationary studies 10
7 Pressure study: 30/100 µm & 3/70 mbar 12
8 Velocity distribution: 30/100 µm & 3/70 mbar 12
9 Simulation: Average channel velocity 13
10 Analytical: Average channel velocity for a square duct 14
11 Reynolds number in the channel of the cell 15
12 Mesh refinement - parametric sweep 16
13 Concentration in the center of the cell vs. delta peak 17
14 Residence Time Distributions for different meshes 18
15 Transient study: Concentration distributions (flow & no flow) . . . 20

1 Introduction

The aim of this project work is to investigate the optimization of mass flow through an electrochemical cell using simulations performed with the program Comsol. Using the cell, voltammetry will be performed on single crystal samples to study catalytic properties of its surface. A typical measurement using the cell may involve the following steps.

1. Prepare sample (surface) in UHV
2. Probe the surface of the sample before measurement using e.g. STM
3. Analyze the catalytic properties using the electrochemical cell (cyclic voltammetry, Differential Electrochemical Mass Spectroscopy (DEMS), Infrared Reflection Absorption Spectroscopy (IRAS))
4. Probe the surface of the sample post measurement

All these steps must be performed without air-exposure to not contaminate the surface. Figure 1 shows a schematic of the flow cell.

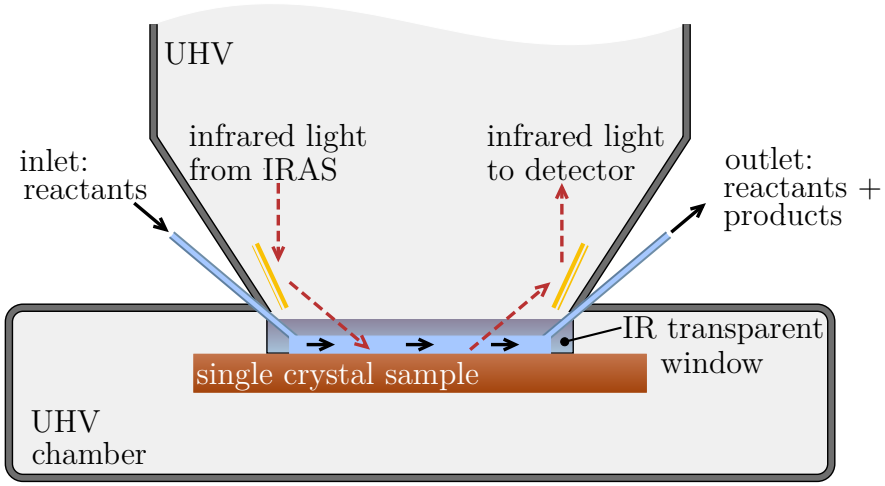

Figure 1: Schematic of a measurement process using the flow cell. Reactants enter from the left, flow over and react with the surface which acts as the working electrode and exit on the other side. The counter- and reference electrode are not drawn in this schematic. During an electrochemical measurement, the surface of the sample is probed using IRAS. Adapted from [1].

It is necessary to be able to detach the flow cell from the sample to prepare measurements on multiple samples taking the four steps listed above. Sealing the fluid against the UHV is realized by pressing the cell against the sample.

The following points [2] must be taken into consideration when designing the cell:

- **Sensitivity** is inversely proportional to the flowrate. Slow flowrates result in low reaction rates (especially if electrode processes are diffusion limited).
- **Time resolution** connects the flow characteristic and geometry of the cell. A good metric to describe the time resolution is given by residence time distributions which will be discussed in Sec. 1.1.4.
- **Uniformity of flow** which means a constant laminar flow in the cell.

Additionally the channel height which is the height of the liquid flowing over the sample must be as thin as possible, with 100 µm being the upper limit [3], to ensure probing with infrared light.

The liquid (electrolyte) is pumped using a vapor pressure driven system as shown in the Figure below to ensure a steady continuous flow across the sample surface.

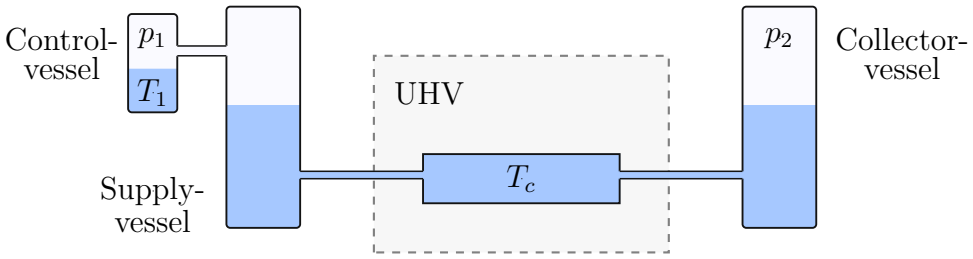

Figure 2: Schematic of the vapor pressure pumping system: The electrochemical flow cell is connected to two reservoirs called *Supplyvessel* and *Collectorvessel* containing reactants and reaction products, respectively. The liquid in these containers is kept on temperature T_c resulting in the pressure p_2 in the *Collectorvessel* on the effluent side of the cell. The *Supplyvessel* containing the reactants flowing into the cell is connected to the smaller reservoir called Controlvessel on the left, partially filled with a fluid kept at constant temperature T_1 resulting in a vapor pressure p_1. The resulting pressure difference $(p_1 - p_2)$ pushes the reactants through the cell.

The extra vessel on the left in Fig 2, supplying the vapor pressure p_1 is necessary to not influence the reaction by keeping the temperature in the flow cell T_c constant.

An estimation of the vapor pressure depending on temperature is given by the Antoine equation:

$$p(T) = 10^{A-B/(C+T)} \tag{1}$$

Figure 3 shows Eq 1 for water with the constants A, B and C being 8.07131, 1730.63 and 233.426, respectively.

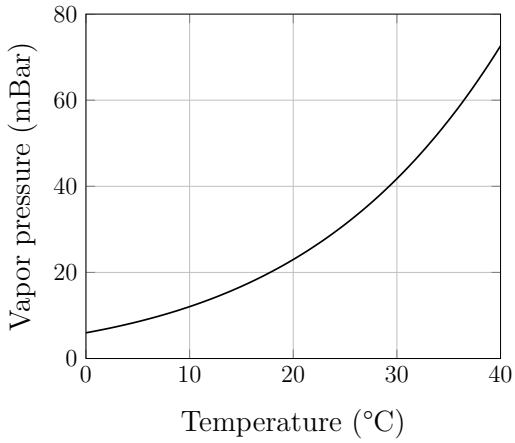

Figure 3: Vapor pressure of water according to the Antoine equation.

1.1 Flow

1.1.1 Reynolds Number

The Reynolds number Re is an important quantity which distinguishes laminar and turbulent flow regimes. It is defined as $Re = uL/\nu$ with u being the average velocity, ν the kinematic viscosity and L the characteristic length. At low Reynolds numbers flow is considered laminar which means uniform smooth flow. Above a critical Reynolds number turbulences arise and the flow gets chaotic and unpredictable. There is also an intermediate state in between laminar and turbulent flow where turbulences start to emerge but are still predictable. This flow is usually called transition flow.

Using the definition of the kinematic viscosity $\nu = \mu/\rho$, the Reynolds number can be written as

$$Re = \frac{uL\rho}{\mu}, \tag{2}$$

in which μ is the so called dynamic of absolute viscosity. The characteristic length depends on the geometry and is usually determined experimentally. For example to characterize flow through a pipe, the inner diameter serves as the characteristic length L.

There are other factors influencing the type of flow described above like the surface roughness and pre-conditioning of the input stream. While roughness and obstacles

of any kind increase the likelihood of turbulences occuring, a well conditioned input stream without inherent disturbances reduces the chance of turbulences. Taking pipeflow as an example, the Reynolds number at which turbulences occur is above around 3000 but may reach values of over 100000 with a well conditioned experimental setup.

1.1.2 Boundary Layers

As a viscous liquid moves across a surface, the molecules closest to the surface adhere to it which is usually denoted as a no-slip condition. Due to molecular cohesion a boundary layer emerges as shown in Fig 4.

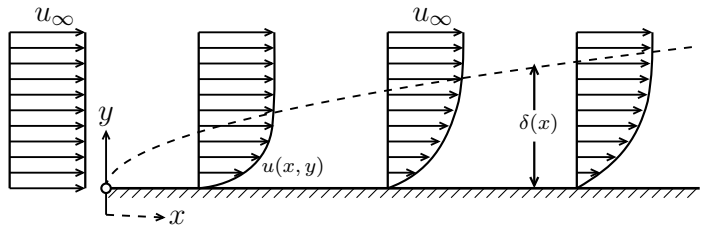

Figure 4: Visualization of boundary layer development over a flat plane. As the unperturbed flow defined by the velocity u_∞ reaches the plate from the left, a boundary layer emerges due to viscous forces in the fluid. The variables $u(x, y)$ and $\delta(x)$ represent the velocity profile and the thickness of the boundary layer, respectively. Adapted from [4].

For laminar flow the thickness of the boundary layer is proportional to the viscosity and can be approximated by [4]

$$\delta = 5\sqrt{\frac{\nu L}{U}} = 5\frac{L}{\sqrt{Re}}$$

where L is the characteristic length and U is the velocity of the unperturbed flow. The thickness $\delta(x)$ usually denotes the distance by which the initial fluid velocity u_∞ decreases by at least one percent, i.e., at distances d greater than $\delta(x)$ the velocity u is greater than $0.99u_\infty$.

This means that for viscous flow in the vicinity of the surface, the fluid velocity changes most.

1.1.3 Darcy–Weisbach Equation

The pressure drop in a channel is proportional to its length L and can be calculated using the Darcy–Weisbach Equation which is given by

$$\frac{\Delta p}{L} = f_d \cdot \frac{\rho}{2} \cdot \frac{\langle v \rangle^2}{D_h} \tag{3}$$

with $f_d = 46/Re$ being the Darcy friction factor and D_h the hydraulic diameter which depends on the geometry of the problem. Taking pipeflow as an example, the hydraulic diameter is the inner diameter of the pipe and for non-circular pipes the hydraulic diameter is defined as $D_h = 4A/P$ where A is the cross-sectional area of the flow and P the wetted perimeter of the cross-section.

For flow in a square duct with width w and height h in which the whole cross-section is filled with the fluid, i.e., no air is transported, the hydraulic diameter is given by

$$D_h = \frac{4wh}{2(w+h)}. \tag{4}$$

1.1.4 Residence Time Distributions

Residence time distributions are useful to describe the behaviour of a system in which mass transports happens. Historically the idea originated from the design of chemical reactors where a chemical inert species is injected at the inlet and the concentration is measured at the effluent side of the reactor. This yields a function of concentration over time $E(t)$, called residence-time distribution function, which acts as a probability distribution when normalized. $E(t)$ gives insight on how much percentage of the injected species spent a certain time in the reactor. Using Residence time distributions various parameters can be derived like for example the first moment gives the mean time t_m a particle of the species has spent in the reactor, which is given by [5]

$$t_m = \frac{\int_0^\infty tE(t)\,dt}{\int_0^\infty E(t)\,dt}. \tag{5}$$

These distributions have found various applications in e.g. Medicine and hydrology. In electrochemistry and especially when researching flow cells, there happens no injection at the inlet and instead the applied voltage acts as a concentration source which will be discussed later on. Since these distributions are dependent on the geometry of the system, they can be used to optimize its shape and form.

1.2 Comsol

To help understand fluid dynamics and electrochemical behaviour of the flow cell, simulations with the finite element program Comsol were performed. All simulations described in this project work were done using COMSOL Multiphysics Version 5.4.0.346.

To run a Comsol simulation, first the geometry of the problem is defined which means creating a (3D) model of the problem we want to solve. Then this geometry is being meshed during which the beforehand created geometry is divided into smaller elements. The next step is setting the physics (equations) which should be solved by Comsol as well as the corresponding material properties and intial/boundary conditions. The last step is performed using a so called study, which can either be a time-dependent or stationary one, depending if the solution changes in time or not. During the study Comsol generates a matrix representing the problem defined by the user and solves it with an algorithm usually denoted the solver. With a successful simulation performed the results can be processed in various ways to extract the desired information.

Both modules used in the simulations of this project work will be described briefly here. The first module is called *laminar flow* and simulates the flow of fluid in the laminar flow regime by solving the Navier–Stokes equations. This module was used because the flow in the cell is expected to be laminar, which will be shown in Sec. 2. The time-dependent form of these set of equations for an incompressible fluid is given by Eq. 6.

$$\begin{aligned} \rho\frac{\partial \mathbf{u}}{\partial t} + \rho(\mathbf{u}\cdot\nabla)\mathbf{u} &= \nabla\cdot\underbrace{[-p\mathbf{I}+\mathbf{K}]}_{\boldsymbol{\sigma}(\mathbf{u},p)} + \mathbf{F} \\ \mathbf{K} &= \mu\Big(\nabla\mathbf{u} + (\nabla\mathbf{u})^T\Big) \end{aligned} \tag{6}$$

In this equation ρ is the density of the fluid, μ its dynamic viscosity, p the pressure, $\mathbf{u}$ the velocity, $\mathbf{I}$ the second order identity tensor, $\boldsymbol{\sigma}(\mathbf{u},p)$ the stress tensor and $\mathbf{F}$ denotes a given external force. For a stationary study the first term $\rho(\partial\mathbf{u}/\partial t)$ in Eq. 6 is zero. Additionally to the Navier–Stokes equations, the continuity equation given by Eq. 7 is solved during a simulation using the *laminar flow* module.

$$\rho\nabla\cdot(\mathbf{u}) = 0. \tag{7}$$

The second module used is called *transport of diluted species*, which solves the convection–diffusion equation given by Eq. 8.

$$\begin{aligned} \frac{\partial c_\mathrm{i}}{\partial t} + \nabla\cdot\mathbf{J_i} + \mathbf{u}\cdot\nabla\mathrm{c_i} &= \mathrm{R_i} \\ \mathbf{J_i} &= -\mathrm{D_i}\nabla\mathrm{c_i} \end{aligned} \tag{8}$$

In this equation c_i is the concentration of the species i, $\mathrm{D_i}$ is the diffusion coefficient, $\mathbf{u}$ denotes the velocity field the species is moving with and $\mathrm{R_i}$ describes source or sink terms. Similarly to the Navier–Stokes equations, the first term $\partial c_\mathrm{i}/\partial t$ is set to zero during a stationary study. The second term $\nabla \cdot \mathbf{J_i}$ describes diffusion with $\mathbf{J_i} = -\mathrm{D_i}\nabla \mathrm{c_i}$ being Fick's first law and $\mathbf{u} \cdot \nabla \mathrm{c_i}$ represents convection terms.

The solution of Eq. 8 for an instantaneous point source in one dimension without convection, i.e., the third term $\mathbf{u} \cdot \nabla \mathrm{c_i}$ being zero is given by [6]

$$\begin{aligned} \mathrm{c_i}(x,t) &= \frac{n_d}{\sqrt{4\pi \mathrm{D_i} t}}\, e^{-x^2/(4\mathrm{D_i}t)} \\ n_d &= \int_{-\infty}^{\infty} \mathrm{c_i}(x)\, dx = \int_{-\infty}^{\infty} \frac{n_d}{\sqrt{4\pi \mathrm{D_i} t}}\, e^{-x^2/(4\mathrm{D_i}t)}\, dx. \end{aligned} \tag{9}$$

In this equation $\mathrm{c_i}$ is the concentration profile of the species i as a function of time and distance from the source and the coefficient n_d is called the source strength which represents the total amount of concentration at any point in time, e.g., the amount of concentration of the initial pulse.

1.2.1 Convergence

Since Comsol usually uses an iterative algorithm to solve the problem, there is always an inherent uncertainty in the solution because the program stops computation when reaching the numerical threshold as defined by the user. Other factors influencing the accuracy of the solution are for example quality of the mesh and the chosen timesteps in case a time-dependent study is done. Since convergence is a key aspect in a Comsol simulation the main ideas concerning convergence are presented below.

- A mesh refinement study should be performed to make sure the mesh is independent of the solution. That means running the same simulation with different mesh sizes and observe the differences of the simulations to determine how much the solution changes. Since simulation time increases with smaller mesh size, the chosen mesh should be as coarse as possible while yielding the desired accuracy for the solution. The observed differences should be taken carefully since it is necessary to interpolate to generate comparable values between different geometries. The interpolation is necessary because Comsol solves the equations on a finite grid.
- For Time-dependent studies it is important that the initial time step the solver takes is representing the physical problem. This step is the first time step the solver takes during a simulation, which by standard is set to a percentage value of the total simulation time. This value is suitable for most

simulations but may not be sufficient to resolve fast changes of the solutions at the beginning. Additionally time stepping should be chosen accordingly to resolve fast changes of the solution. For a time-dependent study the user sets the time steps at which the solution should be given at. By default the time steps taken by the solver are in control of the program. If the solution changes much, the time steps will be shortened and vice versa. The solution will be interpolated to the time values given by the user. This free time stepping is the default setting because it is the fastest and suitable for most cases. There are other options to e.g. force the solver to take time steps defined by the user. In case of doubt, the simulation log should be checked to verify that the solver has taken the correct time steps.

In general the accuracy of a simulation is defined by the user-set tolerance, which stops the solver if the differene beween two consecutive simulation steps have reached the desired value.

Some remarks on runtime optimizations:

- Keep the physical steps separated if possible: In Comsol equations solved are applied through modules with each module containg a set of equations like the Navier–Stokes equations in the molule *laminar flow* as described above. It is possible to apply various numbers of equations and to use multiple modules in a single simulation. If the solution of one module does not depend on the solution of another one it can and should be solved separately. Taking the modules *laminar flow* and *transport of diluted species* as an example. The flow profile from the *laminar flow* module does not interfere with the diluted concentration in the cell. It is therefore possible to solve for the *laminar flow* module separately beforehand without the second module being considered. A second simulation takes the velocity profile from this simulation and applies the module *transport of diluted species* to calculate the spatial concentration over time.
- When using a time-dependent study in conjunction with changing boundary values it is beneficial for the success of the simulation to ramp the parameters instead of changing them instantaneously. That means for example when applying a concentration as a function of a square pulse, to smooth out the shape of the pulse on the rising and falling edge.
- The solution of a stationary can be set as an initial starting point for a time-dependent simulation which may reduce the computation time.

2 Simulations / Results

2.1 Cell Design

To optimize the flow through the electrochemical cell, the design depicted in Fig. 5 has been chosen.

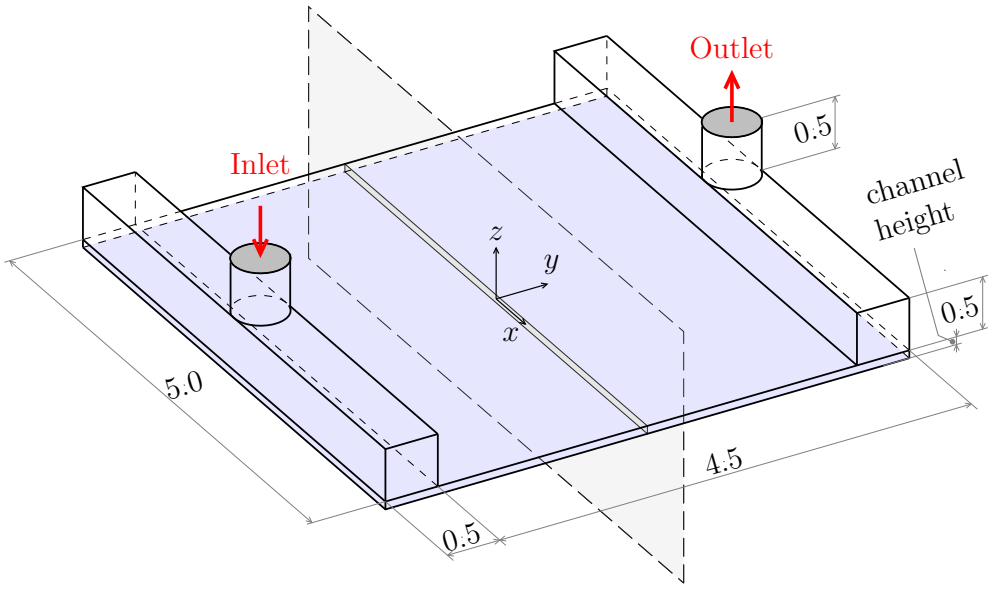

Figure 5: Schematic representation of the flow cell as used in Comsol simulations with all dimensions given in millimeters. Inlet and outlet are marked by gray circles and the direction of flow is indicated through red arrows. The other areas highlighted are the blue one which marks the working electrode and the gray xz-plane in the center of the flow cell which will be used later on.

This schematic directly mirrors the Comsol model which means it only depicts the volume occupied by the fluid. Intially upon creation of the model in Comsol every surface gets a no-slip condition assigned which may be overwritten by the user. That means in Fig. 5 each surface area except inlet and outlet has a no-slip condition applied to. Fluid can only enter and exit trough these surfaces.

2.2 Pressure / Velocity Study

Using the geometry shown in Fig. 5, stationary studies using the module *laminar flow* were done to determine the impact of different channel heights and inlet pressures on the flow properties of the cell. In all simulations water was used as fluid and the outlet was kept at 0 pa while the inlet was set to a certain pressure. Creation of the mesh was left to Comsol defined by one parameter marking the quality of the mesh. This automated meshing considers the ideas presented in Sec. 1.1.2. With the results of these simulations a mesh refinement study was done which is presented in Fig. 6.

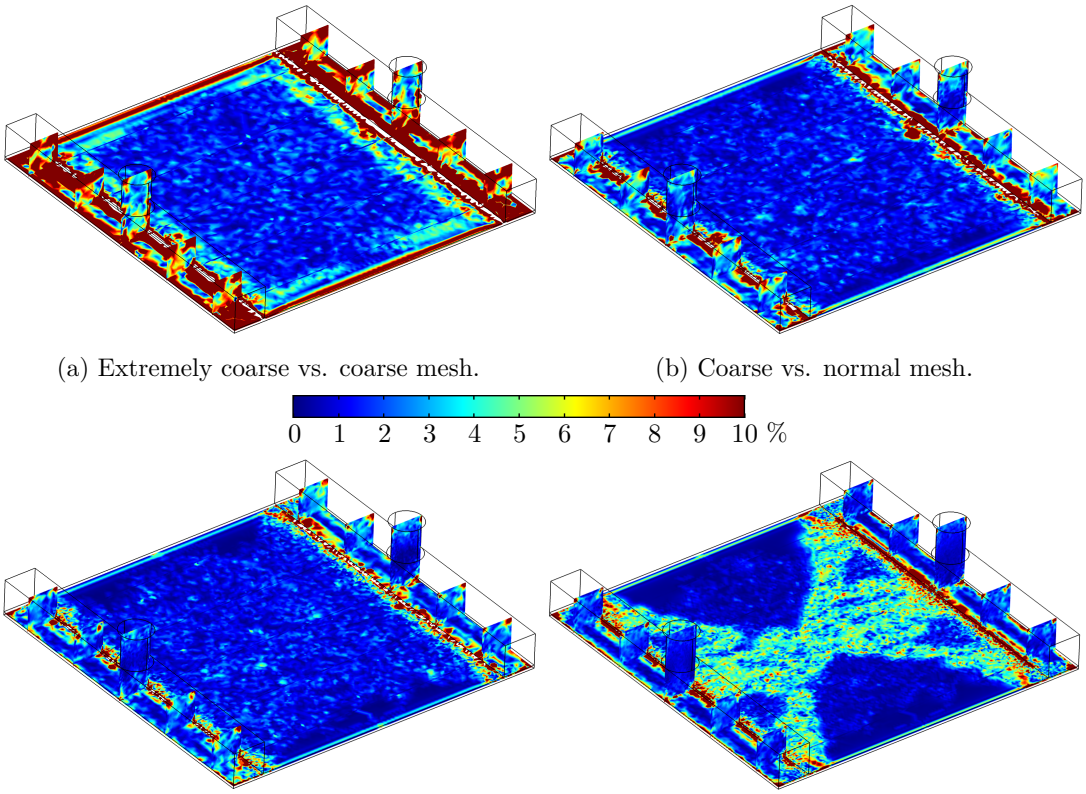

(a) Extremely coarse vs. coarse mesh.

(b) Coarse vs. normal mesh.

(c) Normal vs. fine mesh.

(d) Fine vs. finer mesh.

Figure 6: Mesh convergence study for extremely coarse, coarse, normal, fine and finer meshes. All four figures above display the relative difference in percent of the velocity between two meshes evaluated at six different planes each. For example (d) shows $(|v_{\text{fine}} - v_{\text{finer}}|)/|v_{\text{fine}}| \cdot 100$ with the index indicating the corresponding mesh. The horizontal (x,y)-plane lies is in the middle of the channel and the colorbar applies to all figures.

From Fig. 6 it can be seen that the differences of solutions decrease with the mesh getting more refined which means the velocity is converging against a certain value. A refinement of the mesh yields different improvements on the results depending on the location as can be seen from Figs. 6a and 6b. On the edges there is a big change of the relative difference because the velocity changes most at the edges due to the boundary layer while in the middle of the cell the change is marginal.

Since everything is being solved on a underlying grid (defined by the mesh), the different solutions have to be interpolated by Comsol to calculate the relative difference between of the velocities at certain points. This leads to serveral effects:

- White spots which are clearly visible in Fig. 6a where the fluid enters and exits the narrow part of the channel, caused by a division by zero in the calculation of the relative difference.
- With a different mesh, the objects defining the mesh (in 3D: tetrahedrons, bricks, prisms and pyramids) may change drastically which influences the difference of values observed between meshes as can be seen from Fig. 6d. Comparing different meshes should always be done carefully.

Various informations can be extracted from these stationary studies, which will be discussed below. Since the cell should be as thin as possible to ensure probing with IRAS and the flow will be pressure driven, the main varying parameters are pressure difference and the height of the channel. The pressure at the outlet is always set to zero which means the pressure difference between inlet and outlet is given by the pressure the inlet is set to which will be used further on. On the outlet the flow direction is set perpendicular to the surface which is the standard configuration provided by Comsol. For various channel heights and inlet pressures, stationary simulations were performed with the results of two simulations presented in Fig. 7 exemplarily.

For low inlet pressures, the pressure distribution in the cell follows a strict linear trend with the pressure varying between the inlet and outlet pressure as can be seen from Fig. 7a.

At higher inlet pressures the fluid stream coming from the inlet hits the surface of the sample which produces an area of high pressure which exceeds the value of the inlet pressure, followed by a small region of low pressure in flow direction as can be seen in Fig. 7b

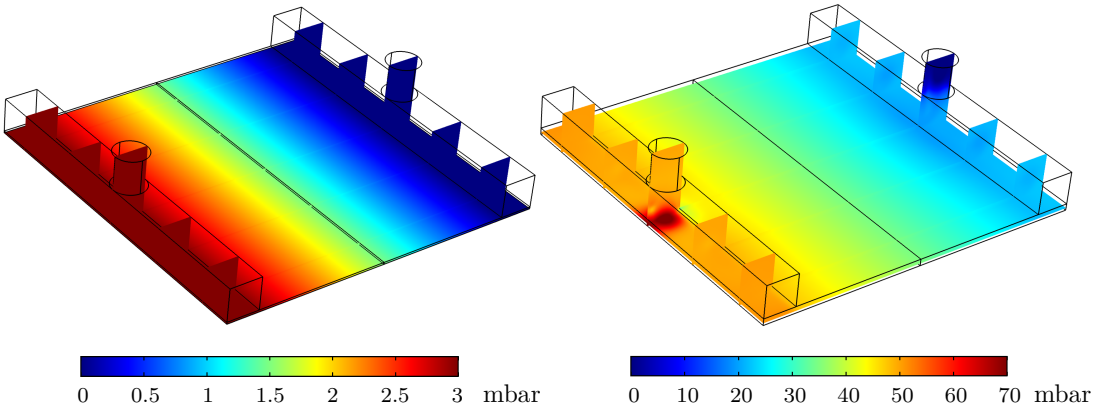

(a) Inlet pressure = 3 mbar
Channel height = 30 µm

(b) Inlet pressure = 50 mbar
Channel height = 100 µm

Figure 7: Pressure distribution in the cell using a finer mesh. The black lines in the center of the cell mark a cutplane used for post-processing which did not affect the simulations.

Figure 8 shows the magnitude of the fluid velocity on a selection of surfaces as well as a some streamlines. A streamline visualizes the trace a particle moves along when released at a given point at the inlet.

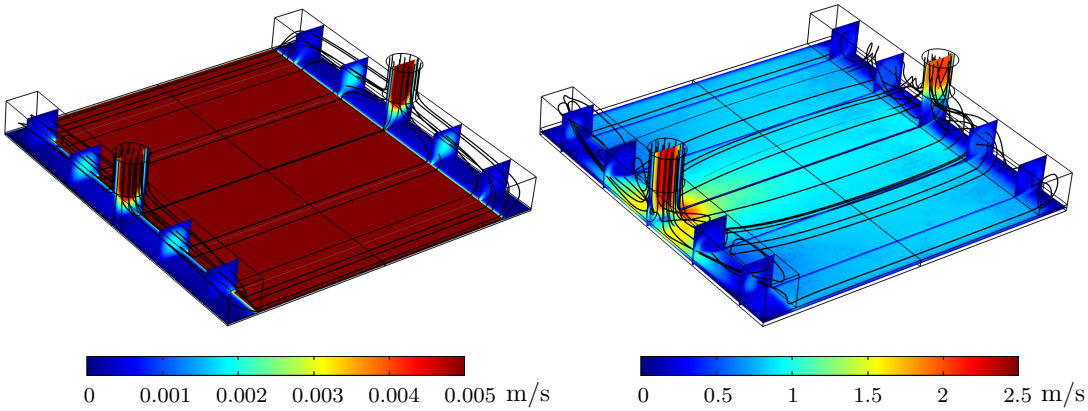

(a) Inlet pressure = 3 mbar
Channel height = 30 µm

(b) Inlet pressure = 50 mbar
Channel height = 100 µm

Figure 8: Velocity distribution in the cell using a finer mesh.

For lower input pressures the fluid velocity is highest in the channel, inlet and the outlet. In the compartments before and after the channel narrowing, the fluid velocity is lowest due to the big cross section as can be seen from Fig. 8a.

For higher inlet pressures displayed by Fig. 8b the fluid slows down as it hits the

wall directly below the inlet and a small area of low velocity emerges. Around this area of low velocity the fluid speeds up locally in flow direction which follows bernoullis principle which states that $v^2\rho + 2p = const$ when neglecting height terms, as can be seen when comparing Figs. 7b and 8b.

The streamlines change drastically when the inlet pressure gets higher. They are no longer parallel in the channel but bent outwards. The flow is also more chaotic in the squares connecting the inlet and outlet tubes with the flow channel.

Using Comsol a so called parametric sweep was performed which means that simulations were done with certain parameters being varied in set ranges. For any combination of the following parameters, simulation were performed to determine the pressure and velocity distributions in the cell.

Channel height: 10, 15, 30, 50, 75, 100 µm
Inlet pressure: 1, 1.5, 3, 5, 10, 50 mbar

Figure 9 shows a contour plot of the average fluid velocity in the channel resulting from the parametric sweep.

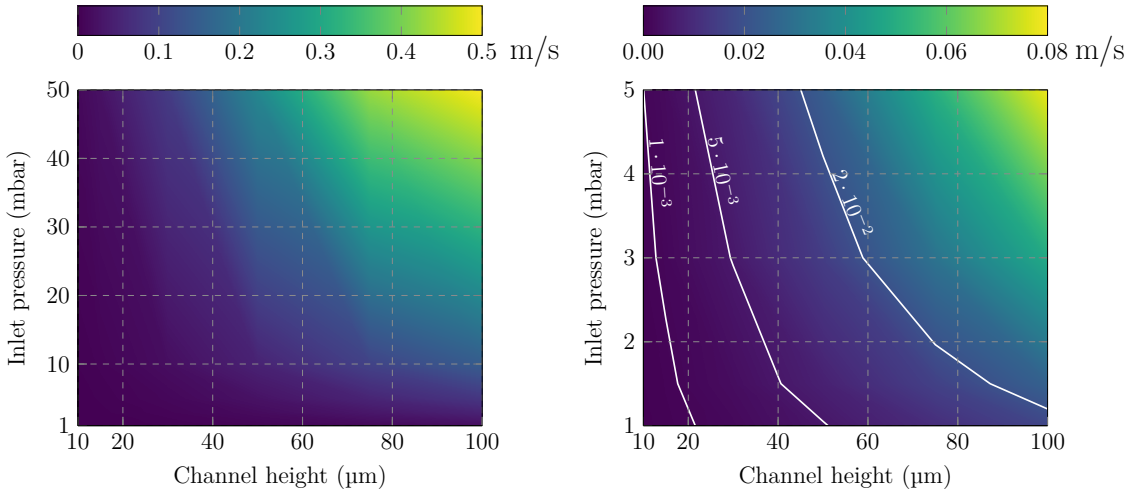

Figure 9: Average channel velocity for channel height and inlet pressure variation. The area over which the velocity has been averaged lies directly in the center of the cell (gray surface highlighted in Fig 5). While a) shows the full range of pressure variation, b) gives a more detailed overview of the channel velocities at lower inlet pressures.

A simplified analytical model is used to validate the Comsol simulations. Using Eqs. 2 and 3, the average velocity in a channel of length L with a hydraulic diameter

D_h caused by a pressure drop Δp can be written as

$$\langle v \rangle = \frac{{D_h}^2}{32 \mu L} \Delta p. \tag{10}$$

To match the simulations, the length of the channel as well as the applied pressure were both scaled by a factor of a half because the simulations are evaluated in the center of the cell. Figure 10 shows Eq. 10 with the dynamic viscosity μ set to 10^{-3} Pa s which is the value for water at 20 °C.

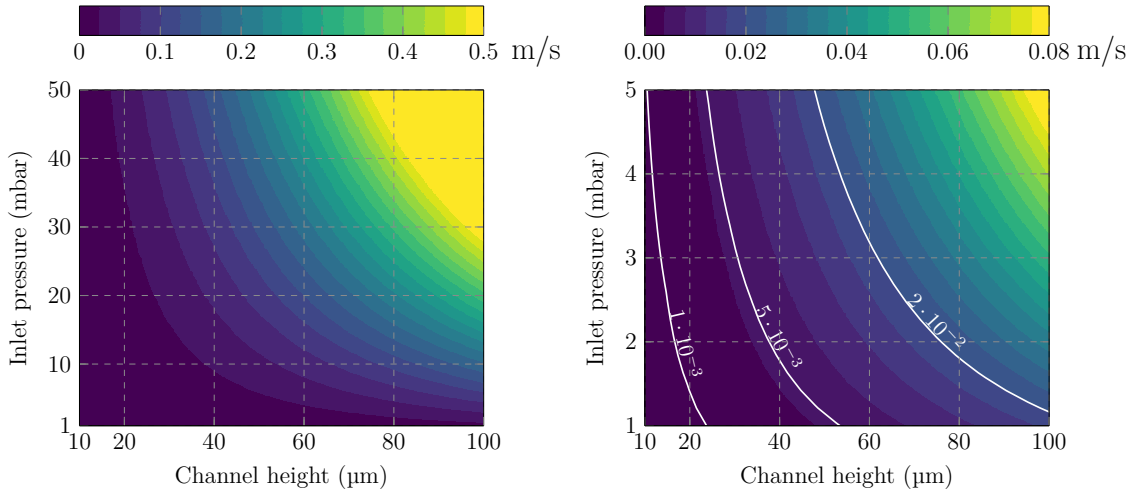

(a) (b)

Figure 10: Average channel velocity in a square duct according to Eqs. 4 and 10 with both channel length L and pressure difference Δp scaled to be able to compare the values with the simulations. See text for details.

The simulations match the analytical solution as can be seen from Figs. 9 and 10. For higher input pressures and higher channel heights, the analytical solution differs from the simulations probably due to the sparse data points and the nature of the simplifications in Eq. 10, i.e., the whole cell is assumed to be a square duct. The general trend of the average velocity getting bigger with increasing channel height and inlet pressure can be explained using the concept of boundary layers caused by the viscosity of the fluid. The liquid moving directly along the wall is slowed down most and this slowing down is proportional to the circumference of the channel divided by its area because the fluid velocity is averaged over the area of the channel. Since the value of this fraction increases with decreasing channel height, the impact of frictional forces increases and the average velocity in the channel therefore decreases.

Despite the good agreement of the simulations with the analytical solution given

by Eq. 10, one should always keep in mind that the solution is more of an estimate since the entire cell is represented by a square channel, which is likely to result in a higher deviation for a more complex cell geometry.

By using the average velocity in the channel and the hydraulic diameter D_h as the characteristic length, the Reynolds number can be calculated using Eq. 2, which is shown as a contour plot in Fig. 11.

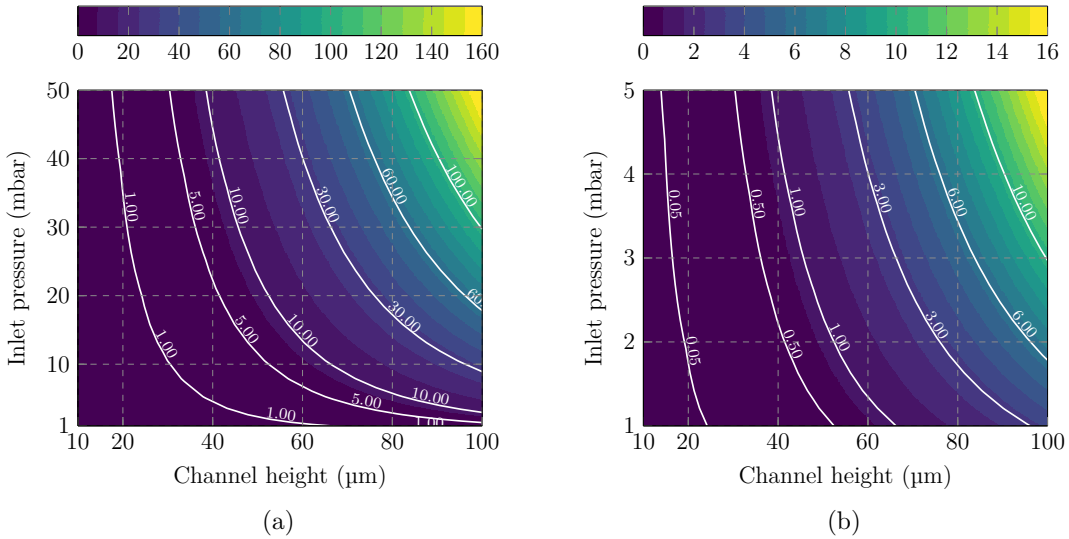

(a) (b)

Figure 11: Reynolds number in the channel of the cell for variation of inlet pressure and channel height.

The Reynolds number increases with increasing channel height and inlet pressure as can be seen from Fig. 11 which is to be expected since the Reynolds number is proportional to the average velocity which follows the same trend. The critical Reynolds number for turbulent flow in a square microchannel with a channel height of 100 µm is around 1200 [7] which means the flow in the cell is laminar since the maximum Reynolds number is around 150 for the scope of the simulations. Nevertheless, it should be noted that the velocity used to calculate the Reynolds number is the average velocity in the channel and that no surface roughness was considered. Despite these two considerations the flow is to be expected laminar only.

The impact of the used mesh on the average channel velocity is shown in Fig. 12.

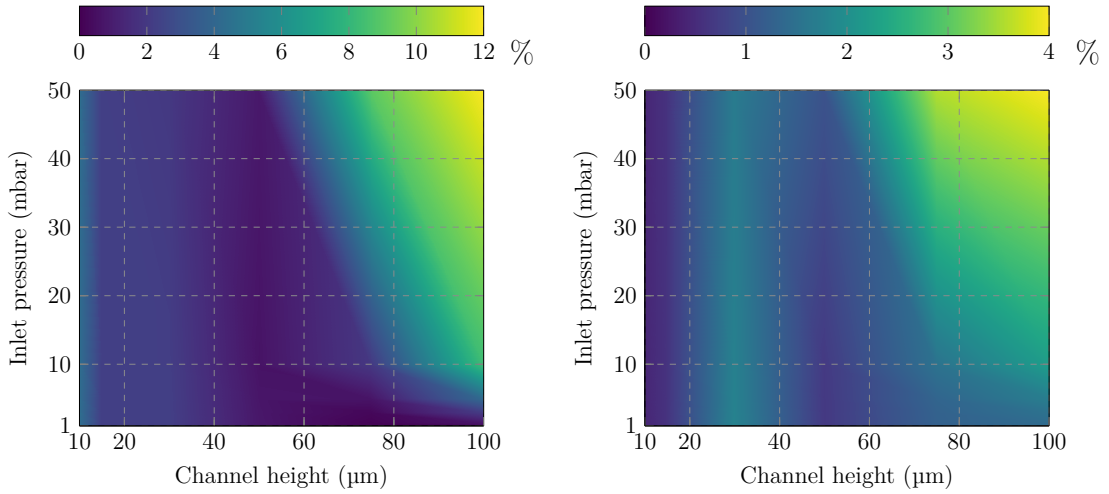

(a) extremely coarse vs. normal mesh.

(b) normal vs. fine mesh.

Figure 12: Mesh refinement study for extremely coarse, normal and fine meshes. The relative change of the average velocity in the middle of the cell is displayed. For example b) shows $|(\mathrm{v_{normal}} - \mathrm{v_{fine}})/\mathrm{v_{fine}}| \cdot 100$ with v being the average channel velocity and the index indicating the corresponding mesh.

With a more refined mesh the percentage difference between the average velocity decreases as can be seen from Fig. 12 but these plots only give information about average values. Local velocity changes are not resolved and therefore these figures should be considered carefully.

2.3 Mass Transport Study

The final electrochemical cell will be operating using an electrode setup which means an electric current between the counter electrode and the working electrode (sample surface) will be applied, reaction products will be created and moved out of the cell. To get a first insight on the mass transport in the cell, simulations with the Comsol module *transport of diluted species* were performed. Using this module a flux defined by

$$J = \frac{3 \cdot 10^{18}}{N_A t_p} \cdot rect[\,] \tag{11}$$

is applied at the surface where the sample connects (light blue surface in Fig. 5) for the duration of a square pulse denoted $rect[\,]$ which resembles the definition in Comsol. That means for times $0 < t < t_p$ the function $rect[\,]$ is one and at any

other time it is zero, with t_p set to 1 ms. N_A is the Avogadro constant and 10^{18} is the number of sulfate ions adsorbed per square meter on a Pt(111) surface [8]. Therefore this set flux simulates the voltage pulse as a total release of a monolayer adsorbed species and the short time duration of the pulse resembles the method fast-scan voltammetry. This influx of concentration is transported through and out of the cell by the velocity caused by the pressure difference. Comsol is able to calculate the concentration of the injected species at any time and point in space. The mass transport can therefore be observed and results of these simulations will be discussed below.

Simulations with the flux defined in Eq. 11 were performed and the concentration in the cell for times $0 < t < 1$ seconds was recorded. The inlet pressure and channel height were set to each 30 mbar and µm, respectively. The diffusion coefficient was set to $10^{-9}\,\mathrm{m}^2/\mathrm{s}$ which is a good estimate for diffusion processes in liquids.

To be able to compare the simulations against the analytical solution given in Eq. 9, the concentration on the surface in the middle of the cell perpendicular to the flow direction (gray surface highlighted in Fig. 5) was taken at certain time steps. The concentration values were averaged over the x-axis which yielded concentration values along the direction perpendicular to the surface the flux is applied to which is presented in Fig. 13.

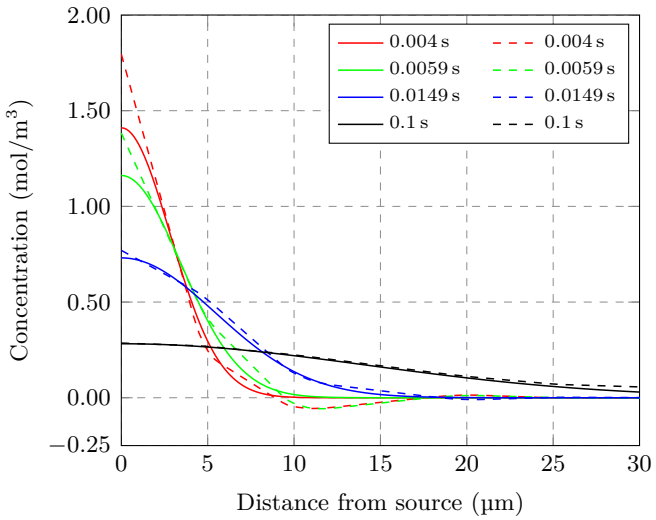

Figure 13: Concentration in the center of the cell from simulations versus the solution of the diffusion equation of a delta peak for four different times. Solid lines represent the analytical solutions according to Eq. 9 and the dashed lines the simulations. While the y-axis displays the concentration, the x-axis represents the distance from the electrode, i.e., the distance from the electrode where the square pulse is applied to.

The source strength n_d is given by the area of the delta peak which is in our case the area of the pulse defined by

$$n_d = 2 \cdot \left(\frac{3 \cdot 10^{18}}{6 \cdot 10^{23} \cdot 10^{-3}} \right) \cdot 0.001 = 1 \cdot 10^{-5}.$$

The factor of two is necessary becaues the solution of the delta peak is symmetric which means that the solution defined by Eq. 9 propagates to both sides. In our case the concentration can only diffuse towards one side and the other is occupied by the source surface.

The simulation is in good agreement with the analytical solution which can be seen from Fig. 13.

By plotting the average concentration at the outlet as a function of time, residence time distributions as described in Sec. 1.1.4 can be generated. A total time of one second was simulated and these results are shown in Fig. 14.

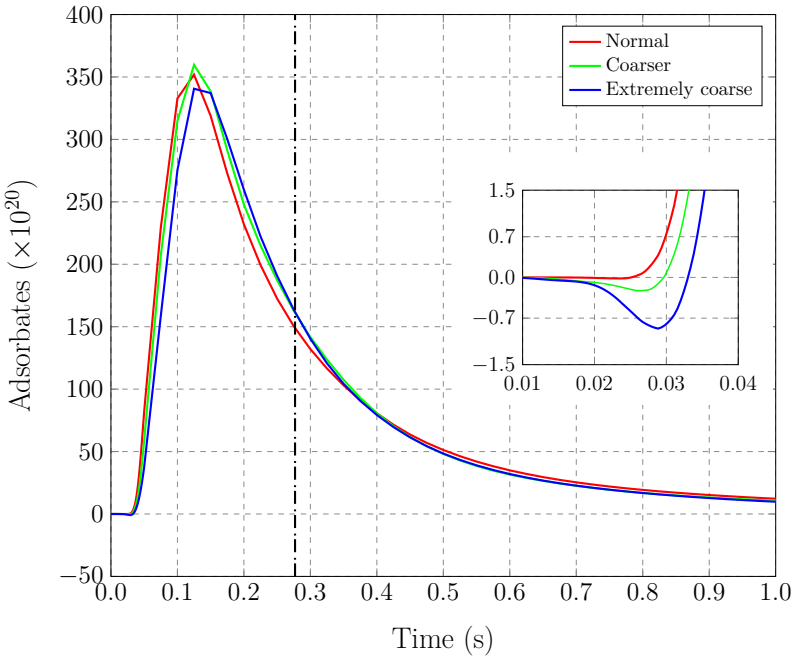

Figure 14: Residence Time Distributions for different meshes. The vertical dash-dotted line marks the mean residence time t_m calculated according to Eq. 5 by numerical integration via trapezoidal rule. Since the mean residence times for all three different meshes are close together, the average value for all three has been drawn. The inset shows the area where the concentration measured at the outlet starts to increase.

The mean residence time t_m for the different meshes are:

Mesh	Mean residence time τ
Extremely coarse	0.278690759719
Coarser	0.273349030603
Normal	0.278771523831

The chosen mesh has little impact on the residence time distribution and the mean residence time as can be seen from Fig. 14. With the exception of the rising edge (see inset Fig. 14), all three meshes yield very similar results which is to be expected since the average of the concentration is considered.

Using Eq. 10 the average velocity in the center of the cell simulated is 47.64 mm/s. Using this velocity and the geometry of the cell (see Fig. 5) we can predict that the first concentration should reach the area defined as the outlet in around 0.021 seconds which corresponds to a distance of 1 mm traveled. The last concentration should exit the outlet at around 0.126 seconds which marks the apex of the time distributions presented in Fig. 14 and represents a distance of 6 mm traveled.

Various insights on the characteristics of the flow in the cell can be connected to the residence time distributions since they depend greatly on the geometry of the cell as well as the flow rates. The amount of concentration at any time in the cell can be calculated by integration over the desired times. The tail beyond the peak in Fig. 14 is therefore proportional to concentration residing in the cell for a certain time, with the length of the tail being proportional to the residing time of the concentration. With that in mind these distributions can be used to optimize the geometry of a flow cell [2].

The time steps set in the simulations can be seen in Fig. 14. To resolve the square pulse, the time steps for the first 0.1 seconds were set closer than the rest of the simulation. As explained in Sec. 1.2.1, this was done to speed up the simulations but did not significantly affect the results.

Using time-dependent simulations in Comsol the concentration at any spatial point at any simulated time step can be visualized. Figure 15 shows the concentration distribution in a cutplane evaluated at various time steps.

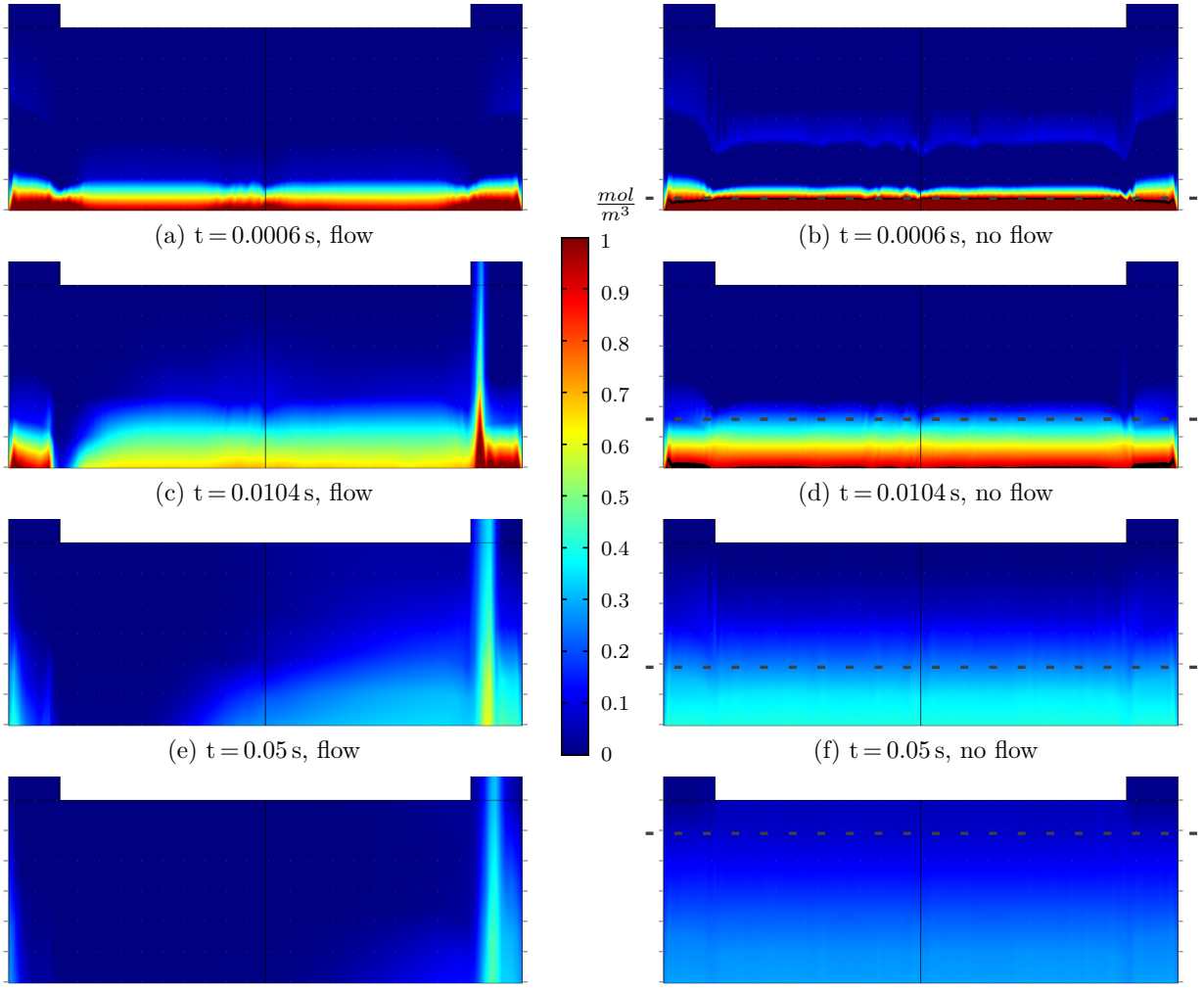

(a) t = 0.0006 s, flow (b) t = 0.0006 s, no flow

(c) t = 0.0104 s, flow (d) t = 0.0104 s, no flow

(e) t = 0.05 s, flow (f) t = 0.05 s, no flow

(g) t = 0.1 s, flow (h) t = 0.1 s, no flow

Figure 15: Concentration distributions at different time steps for a time dependent study. In all eight subfigures only the flow channel is displayed and the top of the cell (cylindrical inlet and the the square parts connecting inlet and the channel) is truncated. Additionally all subfigures are rescaled to map the high aspect ratio of the flow channel. The inflow of liquid happens on the top left and the outlet is on the top right side. While the left column represents a study with applied inlet pressure, i.e., mass is flowing through the cell from inlet to outlet, in the right column there is no applied pressure of any kind and all mass transport is only governed by diffusion. The colorbar applies to all subfigures.

Comparing the two colums in Fig. 15 it can be seen that with applied inlet pressure and resulting flow, mass gets transported out of the cell faster. The four subfigures on the right have a thick dashed horizontal line drawn which marks the diffusion length L which defines the average distance a particle diffuses after a given time t. This distance is given by [9]

$$L = \sqrt{\langle r^2 \rangle} = \sqrt{2nDt} \tag{12}$$

with n being the spatial dimension (here 3) and D the diffusion coefficient. The representation of L in terms of a concentration yielded by the simulation is displayed as a black slice in Figs. 15b and 15d. This highlighted slice marks a concentration of $0.95 < c < 1.05$ with the total concentration in the cell varying between zero and two mol/m^3. This slice recedes after the square pulse is applied which can be seen in Fig. 15d. Therefore the dashed line representing L only matches this concentration slice for small times after the pulse because Eq. 12 does not account for the pulse and assumes a constant concentration for all times greater than zero.

The subfigures on the left of Fig. 15 show the mass flow through the cell in the center slice of the cell for an applied inlet pressure. There are two zones directly below inlet and outlet where concentration resides in the cell for a long time and does not get transported out. The mass in these areas contribute to the long tail of the residence time distributions presented in Fig. 14. This lingering of concentration is a direct result of the cell geometry which can be seen from carefully examining the streamlines in Fig. 8a.

3 Conclusions

Utilizing the program Comsol, simulations were performed to investigate the flow and mass transport in an electrochemical cell. Using stationary studies and the laminar flow module, the velocity and pressure distributions for different inlet pressure and channel geometries has been determined. Time dependent studies using the additional module transport of diluted species were performed to study the transport of matter via diffusion and convection in space and time. From these simulations, residence time distributions were extracted which are useful to evaluate the performance of mass transport in the cell depending on its geometry. The simulation results were tested and verified using analytical models.

Simulations in this project work were performed with a simplified model. The real form is obtained by optimization and changing the geometry utilizing the methods described in this work. Some of these changes are the optimal position of a detection hole for DEMS and adding charge transport as well as the position of the electrodes. Finally, this will be concluded with the production of the cell.

Bibliography

[1] G. S. Parkinson, "Evolving single-atom catalysis: Fundamental insights for rational design," 2019.

[2] V. Shkirskiy, P. Maciel, J. Deconinck, and K. Ogle, "On the time resolution of the atomic emissionspectroelectrochemistry method," *Journal of The Electrochemical Society*, vol. 163, pp. C37–C44, 2016.

[3] F. Faisal, C. Stumm, M. Bertram, T. Wähler, R. Schuster, F. Xiang, O. Lytken, I. Katsounaros, K. J. J. Mayrhofer, M. A. Schneider, O. Brummel, and J. Libuda, "Atomically-defined model catalysts in ultrahighvacuum and in liquid electrolytes: particlesize-dependent co adsorption on ptnanoparticles on ordered co3o4(111) films," *Phys Chem Chem Phys.*, vol. 20, pp. 23702–2371, 2018.

[4] H. S. (Deceased) and K. Gersten, *Boundary-Layer Theory*, p. 26. Springer, fourth ed., 1979.

[5] H. S. Fogler, *Elements of Chemical Reaction Engineering*, p. 879. Pearson Education, fourth ed., 2006.

[6] R. W. Balluffi, S. M. Allen, and W. C. Carter, *Kinetics of Materials*, p. 85. John Wiley and Sons, second ed., 2005.

[7] M. K. S. Verma and V. Kumaran, "A multifold reduction in the transition reynolds number, and ultra-fast mixing, in a micro-channel due to a dynamical instability induced by a soft wall," *J. Fluid Mech.*, vol. 727, pp. 407–455, 2013.

[8] B. Braunschweig and W. Daum, "Superstructures and order-disorder transition of sulfate adlayers on pt(111) in sulfuric acid solution," *Langmuir*, vol. 25, pp. 11112–11120, Sept. 2009.

[9] H. C. Berg, *Random walks in biology*. Princeton University Press, 1993.